Decomposition and Modelling of the BC87 Dataset

Alan G. JONES, Ross W. GROOM,* and Ron D. KURTZ

Geological Survey of Canada, 1 Observatory Crescent, Ottawa, Ontario, Canada, K1A 0Y3

The BC87 data exhibit distortions due to three-dimensional structures at almost all scale sizes from that of the electrode array (<100 m) to that of the 150×50 km plutonic Nelson batholith. These distortion effects must be identified and removed, as far as possible, prior to interpretation. A galvanic model of these distortions is shown to be valid for most of the frequency range of observation, but 3D induction is significant at certain sites for some bands. A first-order regression was fit to the decomposition recovered long period E-polarization apparent resistivities to correct for the remnant local site "static shifts".

We model the distortion- and level-corrected data using both 2D forward trial-and-error fitting and Occam2 smooth inversion. The crustal section of the resulting models correlates well with some geological features. However, the long period phase difference between the E- and B-polarization lasting for more than a decade is difficult to interpret without recourse to introduction of a layer with differing electrical conductivity in the two orthogonal horizontal directions, i.e., an anisotropic layer. There is greater than an order of magnitude difference in the conductivities, with the higher value in conductivity being in a direction which is commensurate with the Juan de Fuca plate-push direction.

1. Introduction

The BC87 dataset (JONES, 1993) consists of magnetotelluric (MT) data acquired at twenty-seven locations along a 150 km east-west transect in 1987 as part of the LITHOPROBE (CLOWES *et al.*, 1993) Southern Cordilleran Transect investigations in British Columbia, Canada. The reader is referred to JONES (1993) for tectonic and geological background information, and for an MT site location map.

These data display three-dimensional (3D) effects at all scales, from that of the electrode array at the site (<100 m), to that of the 150×50 km Nelson batholith, to the regional scale (see Figs. 5 and 6 in JONES, 1993). In appropriate period bands it is possible to characterise these effects as induction in a 2D regional structure with surficial 3D galvanic distortion; a model first suggested by BAHR (1984). After fitting the data from each site in those bands to local galvanic distortion models, we model the data in those frequency bands that we consider are representative of the 2D regional structure using both forward trial-and-error fitting and a regularized smooth inversion scheme (DEGROOT-HEDLIN and CONSTABLE, 1990). Herein, we report briefly on our distortion analyses, and our 2D forward and preliminary inversion models. Two papers in preparation (GROOM *et al.*, 1994; JONES *et al.*, 1994) will go into more details of the former, and will present and discuss our finalized inversion models and their tectonic implications.

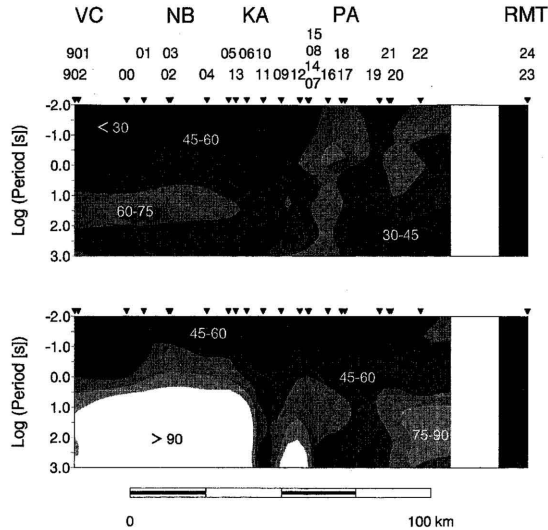*Now at: Department of Geological Sciences, Queen's University, Kingston, Ontario, Canada.

Fig. 1. Phase pseudosections of the raw ϕ_{xy} (top) and ϕ_{yx} (bottom) phases in a geographic co-ordinate system with x north. The contour interval is 15°; black regions denote phases below 30°, whereas white regions denote phases greater than 90°. The locations of the main geological structures are indicated: VC - Valhalla Gneiss Complex; NB - Nelson Batholith; KA - Kootenay Arc; PA - Purcell Anticlinorium; RMT - Rocky Mountain Trench (see JONES, 1993).

2. Data

The recorded MT data exhibit strong site to site variations across the entire line. Even sites as close as 1 km to each other, e.g., *lit007* and *lit008* (JONES and GROOM, 1993), show very different MT impedance tensors which cannot be reconciled with their proximity without introducing significant local galvanic distortion. GROOM *et al.* (1993) show in detail that careful analysis of data from sites *lit902* (named *litw02* in that paper) and *lit000*, which initially appear disconguent, reveals a common regional strike direction. Traditional 2D techniques give a strike which varies strongly from site to site. However, the recorded data suggests a broad regional response partially masked by strong 3D scattering effects. As an example, the phases of the off-diagonal elements are given in Figs. 1a (Z_{xy}: quasi-"E-polarization") and 1b (Z_{yx}: quasi-"B-polarization") for impedance tensors which were measured in, or rotated to, a geographic north-south/east-west coordinate system (the site locations have been projected onto a geographic east-west line). As shown previously by JONES *et al.* (1988), one of the most striking characteristics is that for more than 60 km E-W, from the western boundary (site *lit000*) of the Nelson Batholith to its very eastern edge (site *lit013*), the phase of the Z_{yx} impedance element for all sites rises rapidly to above 90° for periods longer than about 3 s. Some sites on the Purcell Anticlinorium (PA) to the east also have Z_{yx} phases above 90° at very long periods (>100 s). In addition, one will note the strong site to site variations in the phases across the PA particularly in the phase of the Z_{xy} element and at periods longer than about 0.2 s.

Some workers have suggested that induction arrows be used to define the regional strike direction in the presence of strong telluric distortion. For the BC87 data, the induction arrows (not shown) display no distinctive large-scale regional pattern but show instead patterns associated with local structures. For example, in the Kootenay Arc (KA) area (centered about station *lit006*) at periods around 3 s, the reversed real induction vectors point towards the KA (JONES *et al.*, 1988, Fig. 5). These currents we associate with a shallow region of enhanced conductivity

due to lead-zinc-silver disseminated deposits (see Discussion and Conclusions) exposed in the Bluebell mine at Riondel. In addition, as will be shown below from the decomposition analyses, for most stations there is an onset of strong 3D effects between 1 and 10 s period. These 3D effects appear similar over rather large areas and, given the resistivities and periods involved, are most probably due to large structures of the size of the Nelson batholith. At periods where these large structures begin to respond three-dimensionally, not only galvanic electric distortion effects would be expected but also 3D induction and the magnetic effects of galvanic current distortion (GROOM, 1988; ZHANG *et al.*, 1993). Both of these effects will, in general, include a vertical magnetic field that adds to any vertical magnetic field caused by 2D induction on a regional scale. Our experiments with synthetic data indicate that such effects can prohibit the determination of strike direction from the magnetic transfer function data alone. Accordingly, we did not use the transfer function information when determining the strike direction.

3. Decomposition

Although a variety of decomposition techniques were used to examine the data, here we will report on our understanding gained by using Groom-Bailey (GB) decomposition. The assumed model is one of 3D galvanic distortion of a 2D regional response, termed 3D-over-2D (3D/2D). The fundamental theory for this technique is given in GROOM (1988) and GROOM and BAILEY (1989a; herein called GB1), and the technique's relation to some other approaches is given in GROOM and BAILEY (1991; herein referred to as GB2), while a comprehensive explanation of its use in data analysis is given in GROOM *et al.* (1993; herein referred to as GKJB). Additional material may be found in GROOM and BAHR (1992), and JONES and GROOM (1993). The reader is referred to GKJB for a full description of the methodology adopted; a brief description is given below for completeness.

In GB decomposition, the eight data at each frequency are fit to a seven parameter 3D/2D model. One parameter represents the regional 2D strike, two parameters describe principally the phase mixing effects of the galvanic distortions (called *twist* and *shear* by GB1), and the remaining four are the two complex 2D regional impedances scaled by unknown static shift factors. GB1 characterise the shift factors as a single local *site gain*, g, and an anisotropy tensor, A, which splits the two apparent resistivity curves apart. Theoretical studies show that the effect of g is usually small compared to the anisotropy (GKJB). The anisotropy can often be minimized by shifting the ρ_a curves such that their high-frequency asymptotes are that of the geometric mean of their values (GKJB).

Having determined these GB parameters for all frequencies, the next step is to constrain the strike, twist and shear to be frequency-independent, taking into consideration the increase in misfit between the model response and the data with reducing degrees of freedom. The misfit parameter is a normalised χ^2 statistic indicating the misfit of the distortion model at that frequency; values below 4 indicate that the data fit the model to within statistical tolerances (GKJB). The objective is to fit a model of $4N+3$ parameters to the $8N$ data at N frequencies.

Once a frequency- and site-consistent strike is determined, the data must be fit to a distortion model rather than merely rotating the impedance tensors to the desired strike. GKJB and JONES and GROOM (1993) show that this model-fitting procedure gives superior estimates of the 2D regional responses to the ones from rotating the impedance tensor.

3.1 General

In the following we discuss some details of the analysis for two sites, *lit902* and *lit004* chosen for their characteristics which illustrate certain aspects of our approach, and briefly illustrate the GB analysis of several other sites. The data from site *lit902* were chosen because the regional responses can be quite easily recovered once a 3D/2D model is adopted. The data are only distorted

by near-surface local inhomogeneities. In contrast, the data from site *lit004* are representative of all those recorded on the Nelson batholith. Large-scale 3D inductive and galvanic effects, caused by the presence of the batholith itself, cause severe distortion of the phase responses. It is only with careful application of distortion methodology that we are able to extract regional information from these data.

Colour-contoured plots of the type illustrated in GKJB showing the variation of twist, shear, current channelling, error, and a normalised form of the error, were used extensively as an aid in determining the regional strike direction and its frequency and site-to-site variability. One plot, for site *lit902*, is shown herein in grey-scale (Fig. 3b) to illustrate their utility; a colour version of this figure is included in GKJB (Fig. 17 in GKJB).

Although the normalized misfit should be less than 4 for an acceptable model of distortion, this requires reliable error estimates. The estimates in these data were derived using standard spectral analysis procedures, and, in our experience, they are far too small when the number of individual spectral estimates that contribute to the average is large. This is particularly true in the MT "dead-band" where there were typically many hundreds to thousands of individual spectral estimates in the final average. Conversely, the estimates at longer periods are probably too conservative. Accordingly, we placed emphasis on the visual fit of the modelled parameters to the scaled impedances, rather than just on the single misfit value itself.

3.2   Valhalla gneiss complex response (lit902)

Station *lit902* is situated on the Valhalla gneiss complex approximately 15 km west of the Slocan Lake Fault (see Figs. 2 and 3 of JONES, 1993). Figures 2a and b show the model parameters and fit for a best-fitting 2D parameterization. In Fig. 2a notice the gradual increase in the skew (skew is defined here as an angle given by $\tan^{-1}(Swift's\ skew)$) from near zero to about $30°$. Also note the sharp jump in strike from about $35°$ to $85°–90°$ at around 0.3 s. The details of the misfit are given in Fig. 2b, in a scaled fit of the estimated impedance tensor under the GB model compared with the scaled data (GKJB). This 2D parameterization fits the off-diagonal components well, but the diagonal components are not fit after the first few periods; at long periods there is little resemblance between the estimated and actual data. In addition, the minor impedance phase rises above $90°$ at periods greater than 10 s, and the apparent resistivities cross-over just at the break in the estimated strike. Clearly, for this site, and almost all of the others in this dataset, a 2D parameterization neither fits the data nor yields a physically-interpretable response.

GB decomposition was used to seek a best-fitting strike for a 3D/2D model. Figure 3a shows the best-fitting GB parameters and misfit for these data with no constraints applied, and Fig. 3b shows the contoured plots of the GB parameters, as a function of period and strike, for this site. At periods in excess of about 0.1 s the twist becomes frequency-independent with values in the range $15°–17°$, and the strike shows a preference around $60°$, but with some variation which mirrors the variation in shear. As discussed by GB2, GKJB and JONES and GROOM (1993), one, or both, of the telluric distortion parameters is generally more stable than the estimates of strike. Figure 3b displays the values of the Log(error), normalized error (see GKJB), twist, shear, and channelling azimuth as the strike is varied from $0°$ to $90°$. The log(error) plot illustrates that inappropriate choice of strike angle will leads to very large misfit errors. In particular, the inferred strike from a 2D parameterization at periods greater than 3 Hz, of $80°–90°$ (Fig. 2a), leads to virtually the worst misfit (see the normalized error plot), and is, in fact, close to the strike-independent current channelling azimuth (lower right plot of Fig. 3b).

The next step is to constrain one or more of the parameters until a solution is obtained with frequency-independent strike, shear and twist which fits the data as well as possible (step 3.2 in GKJB). However, one must exercise caution when constraining either of the telluric distortion parameters as their value imposes a coordinate system reference frame on the strike determination.

LIT902 2D

(a)
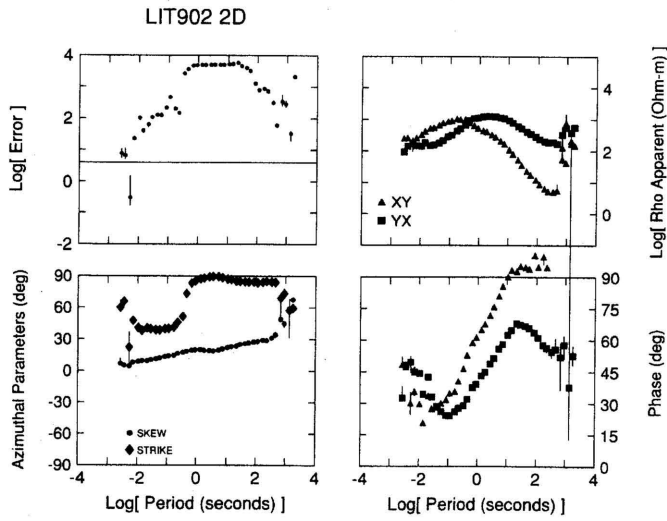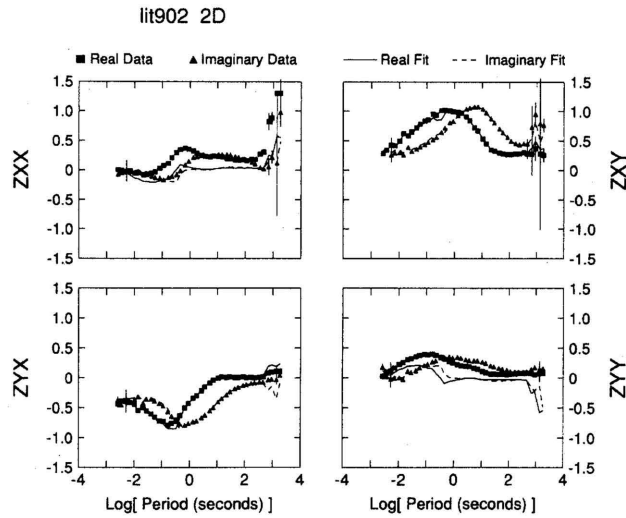
lit902 2D

(b)

Fig. 2. (a) The GB parameters for unconstrained 2D fit to site *lit902*. *Upper left*: Logarithm of the normalized χ^2 misfit; *Lower left*: strike (*diamonds*) and skew (*circles*); *Upper right*: Estimated scaled regional apparent resistivities (the data in the strike direction are denoted XY (*triangles*), whereas the perpendicular responses are YX (*squares*); *Lower right*: Estimated regional phases. (b) Fit of the model data (solid (*Real* parts) and dashed (*Imaginary* parts) lines) to the observed data. (squares: *Real* parts; triangles: *Imaginary* parts) for all four impedance elements; both model and field data are scaled to an appropriate layer over a half-space (see GKJB).
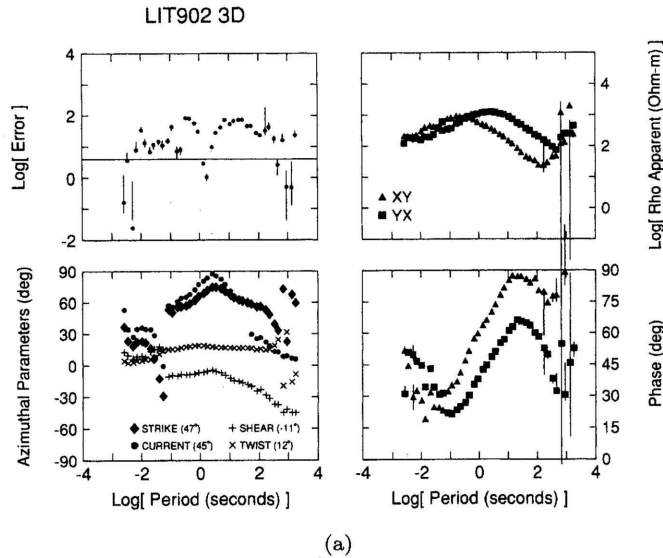
Fig. 3. (a) The unconstrained GB parameters for a 3D/2D model for the data from site *lit902*. All diagrams are as for Fig. 2, with the exception of; *Lower left* GB distortion parameters strike (*diamonds*), shear (*pluses*), twist (*crosses*) and local current channelling (*circles*). The values in brackets after each parameter is the average value over the whole period range.

The contour plots (Fig. 3b) show that in the period range 0.1 s–100 s the lowest model fits are obtained with strikes in the range 55°–70°. Careful examination of the data for strikes in this range revealed that a strike close to 60° was preferred considering all aspects of the decomposition model. Figure 4 shows the parameters obtained with a constant strike direction of 60°; again a twist of 16°–17° is indicated in this period range. Constraining the strike and twist to these angles gives a shear with a preference for around −10°. The final constrained parameters, with strike of 60°, twist of 17°, and shear of −11°, are shown in Fig. 5a with the fits to the scaled impedances in Fig. 5b. The misfit statistic for this 3D/2D model is only marginally different over the 2D model (Fig. 2a) at high frequencies but is significantly improved at longer periods (by greater than an order of magnitude) due to the reduction in the misfit statistic and to the reduction in free parameters for this final constrained model. As can be seen in the fit to scaled impedance elements (Fig. 5b) this model fits all four elements reasonably well, although there is a misfit in the diagonal elements particularly in the yy-component. The minor phase (ϕ_{xy} in this coordinate system) is now below 90° at all but the longest periods (>300 s) and the minor impedance magnitude is not as small as the 2D estimates at long periods.

3.3 Nelson batholith response (lit004)

The plutonic Nelson batholith is bounded by sites *lit013* and *lit000* on its eastern and western borders respectively (Figs. 2 and 3, JONES, 1993). Station *lit004* is in the middle of the batholith, and Fig. 6 illustrates the 2D decomposition of its data. Notice the sharp change in strike, from 45° to 0°, at about 1 s, the minor phase going well above 90 degrees in the long periods, and the large misfits. The minor phase rising out of the quadrant is similar for all sites on or near the batholith, as shown in Fig. 1b and discussed above.

It is possible to find a 2D strike direction that keeps both phases within their respective quadrants (GROOM *et al.*, 1994). Rotating the MT impedance tensor through 180° and deriving $\phi_{xy}(\theta)$ illustrates that for azimuths in the range 61°–123° the phases at periods above 3 s are

lit902

Log(error)

ABOVE 3.0
2.3 - 3.0
1.7 - 2.3
1.0 - 1.7
0.3 - 1.0
-0.3 - 0.3
-1.0 - -0.3
BELOW -1.0

Strike

Normalized Error

Log(Period [s])

Above 15

Below 5

Strike

Twist

45

0

-45

Strike

Shear

Strike

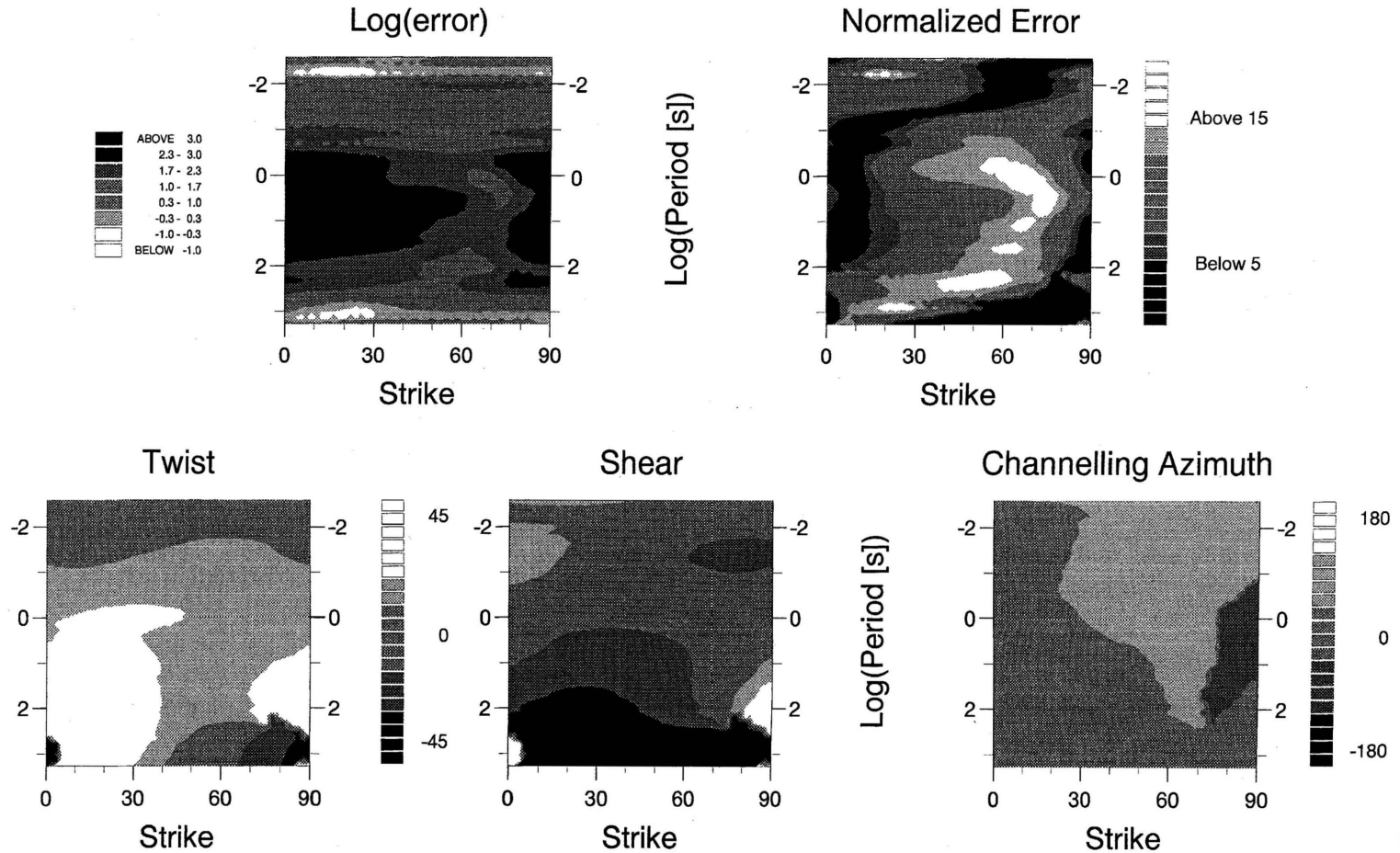## Channelling Azimuth

Log(Period [s])

180

0

-180

Strike

Fig. 3. (b) Grey-scale contour plots of the variation of the decomposition parameters with strike direction from 0° to 90°. The normalized error is a normalized, non-linear, inverted scale (see GKJB); values in excess of 15 (*white*) show strikes which are best-fitting, whereas values less than 5 (*black*) show the worst-fitting strikes.
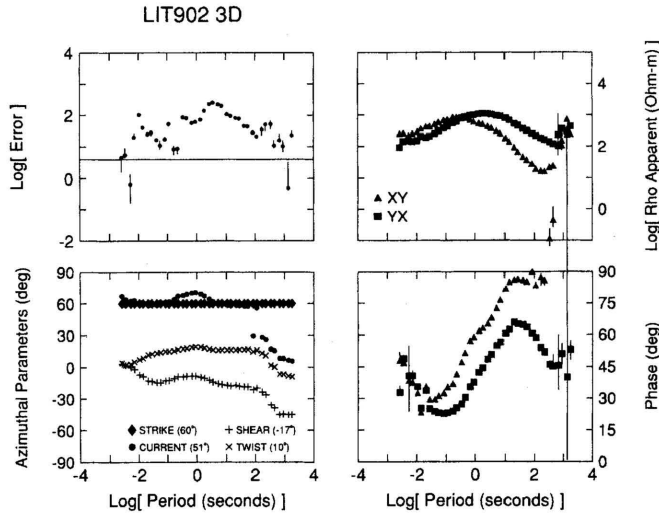
Fig. 4. The 3D/2D GB parameters for site *lit902* with the strike constrained to 60°.

greater than 90°. Such out-of-quadrant phase behaviour is observed for all sites on the batholith, from the eastern end (*lit013*; 59°–125°) to the middle (*lit002*; 57°–136°) to the westernmost (*lit000*; 57°–122°). In contrast, $\phi_{xy}(\theta)$ phases from sites just off the batholith (stations *lit006*, which lies 3.6 km east of *lit013*, and *lit901*, 15.8 km west of *lit000*) remain within the first quadrant regardless of azimuth. There is high sensitivity in the $\phi_{xy}(\theta)$ phase to rotation angle; for example for the data from site *lit000* in the Slocan Valley the phases at periods above 5 s are all greater than 100° in an azimuth of N120°E, but all below 75° in an azimuth of N125°E. Thus a valid regional 2D response can only be found for these batholith sites with a strike direction in an azimuth in the range of 47°–56° (or −43° to −34°). Three-dimensional galvanic distortion will, in general, mix the regional responses (GB1 and GB2), and this mixing is dependent on the coordinate system (i.e., strike) chosen. Here in Fig. 6, we see that in the 2D strike direction this mixing has provided a minor impedance which at long periods is merely a scalar multiple of the major.

Decompositions indicate that a 60° strike is not as well defined for these data as for the data from site *lit902*, but still gives an acceptably low misfit except around 1 s. The azimuths which yield the lowest misfits give physically-unrealisable 2D regional responses (phases out-of-quadrant), which emphasizes the points made in GKJB that it is difficult to automate distortion analysis. Consideration must be given, particularly in the case of severe distortion, to the information from sites with superior statistical properties. For the batholith data, we were guided by the data from the nearby off-batholith sites (see GKJB and GROOM *et al.*, 1994). Figure 7 shows the GB parameters for a fixed strike of 60° as at lit902; note the rapid increase in the twist and shear parameters, from small values to 14° and −38° respectively, beginning at the period where the misfit is greatest and where there is a strong gradient in the 2D strike (Fig. 6). The high value of shear, close to its theoretical limit of −45°, indicates severe current channelling effects at these periods.

GKJB provides a more detailed discussion of this type of analyses which includes the analyses of another site on the batholith (*lit000*) in the Slocan Lake valley. This site has different high frequency characteristics from *lit004* but very similar long period characteristics.

This variation in the parameters indicates that we are moving from one 3D/2D regime at

LIT902 3D (FIXED PARAMETERS)

(a)

lit902 3D (FIXED PARAMETERS)
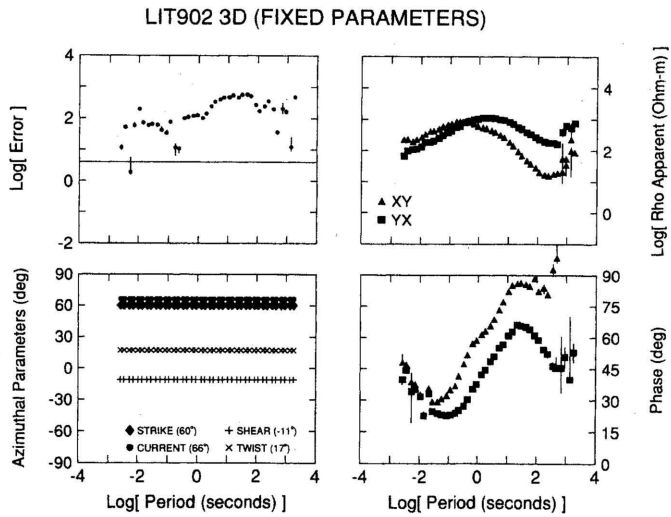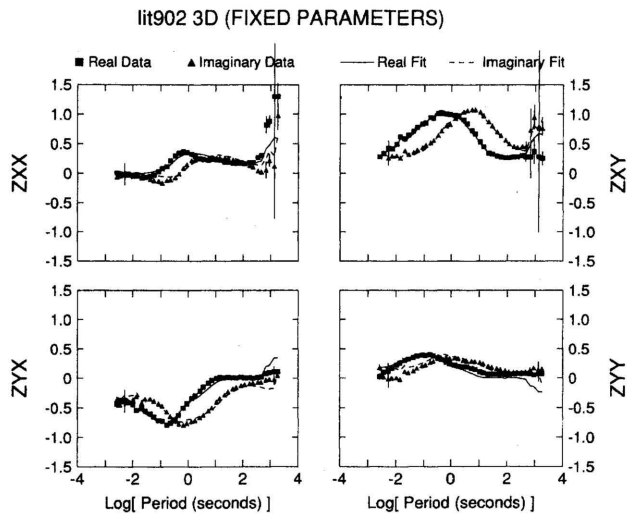
(b)

Fig. 5. (a) The final 3D/2D GB parameters for site *lit902* with strike, shear and twist constrained to 60°, −11°, and 17° respectively. (b) Fit of the model data to the field data.
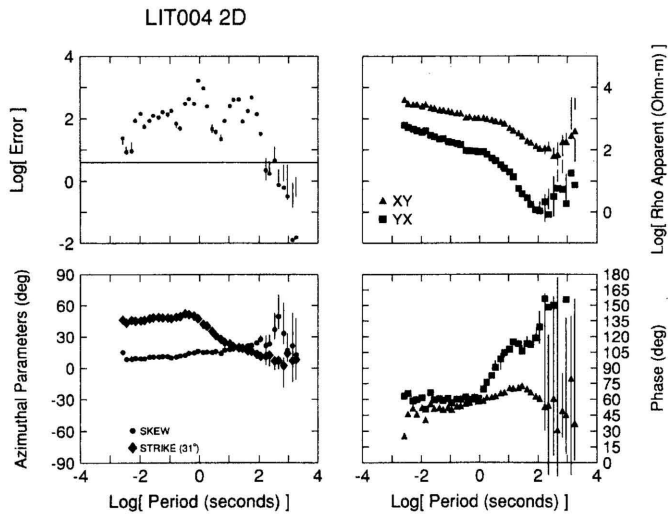
LIT004 2D

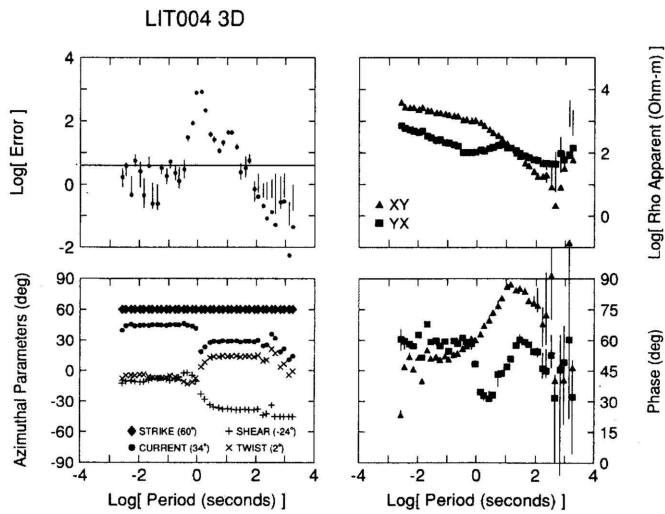Fig. 6.   The GB unconstrained 2D model parameters for site *lit004*.

LIT004 3D

Fig. 7.   The 3D/2D model parameters for site *lit004* with strike constrained to 60°.

short periods (<1 s) to another 3D/2D regime at long periods (approximately >10 s) through a regime in which a 3D/2D model is only an approximate description (GROOM, 1988). It is in this band of 1–10 s that regional-scale 3D distortions become significant, and it should be noted that the periods of onset of these effects are those appropriate for the horizontal scale size of the Nelson batholith (150×50 km), not its vertical dimension (<5 km); the skin depth at 1 s for a resistivity appropriate for the batholith (>10,000 Ω·m) is over 50 km. In addition, the period at which the phase goes out of quadrant for certain azimuths, about 2–3 s, is independent of the location of the site on the batholith. It is the same for sites in the middle where the batholith is at its thickest (5 km) as for those on the boundaries (*lit000* and *lit013*) where it thins to a few hundred metres at most.

As will be discussed below, one aspect we had difficulty in modelling is the large phase difference in the period band 1–10 s between the two modes. This difference is as great as 40° at 3 s. We attribute these responses to 3D magnetic effects (GROOM, 1988; GB1) which exist in this band to the presence of the batholith. We experimented with a variety of 3D modelling programs in an attempt to synthesize these magnetic effects, but were not successful.

3.4   Singular decomposition tensors (lit009)

GKJB have shown that resolution of a regional 2D induction azimuth is highly dependent upon the noise content with respect to the condition number (singularity) of the impedance tensor. In some cases for these data, current channelling is so severe that the impedance tensor is essentially singular to the noise; in which case, only one eigenvalue will be obtained (GB2). Contoured period-strike plots for site *lit009* show that the current channelling azimuth is virtually strike-independent with a value around −82°, which is indicative of severe current channelling. The regional strike does not show a preference for any particular direction. In these cases, once the regional strike is known from neighbouring sites, one of the regional responses can generally be obtained from the decomposition (GROOM et al., 1994).

3.5   Other sites: lit011 and lit017

All the other sites were treated in a similar manner; as examples the unconstrained 3D/2D parameterization models of two of them are shown in Figs. 8a (*lit011*) and 8b (*lit017*) (note the "mode-swap" for the high frequency data compared to the long period data for site *lit017* at 1 s). Site *lit011* lies on the eastern shore of Kootenay Lake at the western edge of the Purcell Anticlinorium (PA), whereas site *lit017* is in the middle of the PA. Site *lit011* shows a strong preference for 60° (or −30°). The longer periods for site *lit017* also show such a strike direction, but at short periods there is the indication of a 0° strike. Fixing the strike direction at 60°, and determining the appropriate twist and shear values, leads to constrained GB parameters shown in Fig. 9 with the fits of the model parameters to the data shown in Fig. 10. Although the constrained models have larger misfits than the unconstrained ones, the data are well explained. These large misfits arise from error estimates that are too small, rather than departures from the validity of a 3D/2D model (GKJB; GROOM et al., 1994).

4.   Site Gain Determination

The decomposition analyses revealed that, apart from the 90° ambiguity, −30° appears to be appropriate for all but a few stations as the regional strike direction. We chose −30° as the strike direction (i.e., TE or E-polarization) rather than +60° based on the surface trends of the major morphotectonic belts (see JONES, 1993). After fixing this as the strike direction for the dataset, the GB model, with frequency-independent twists and shears, was fit to the data from each site to determine the scaled regional 2D impedances (GKJB; JONES and GROOM, 1993).
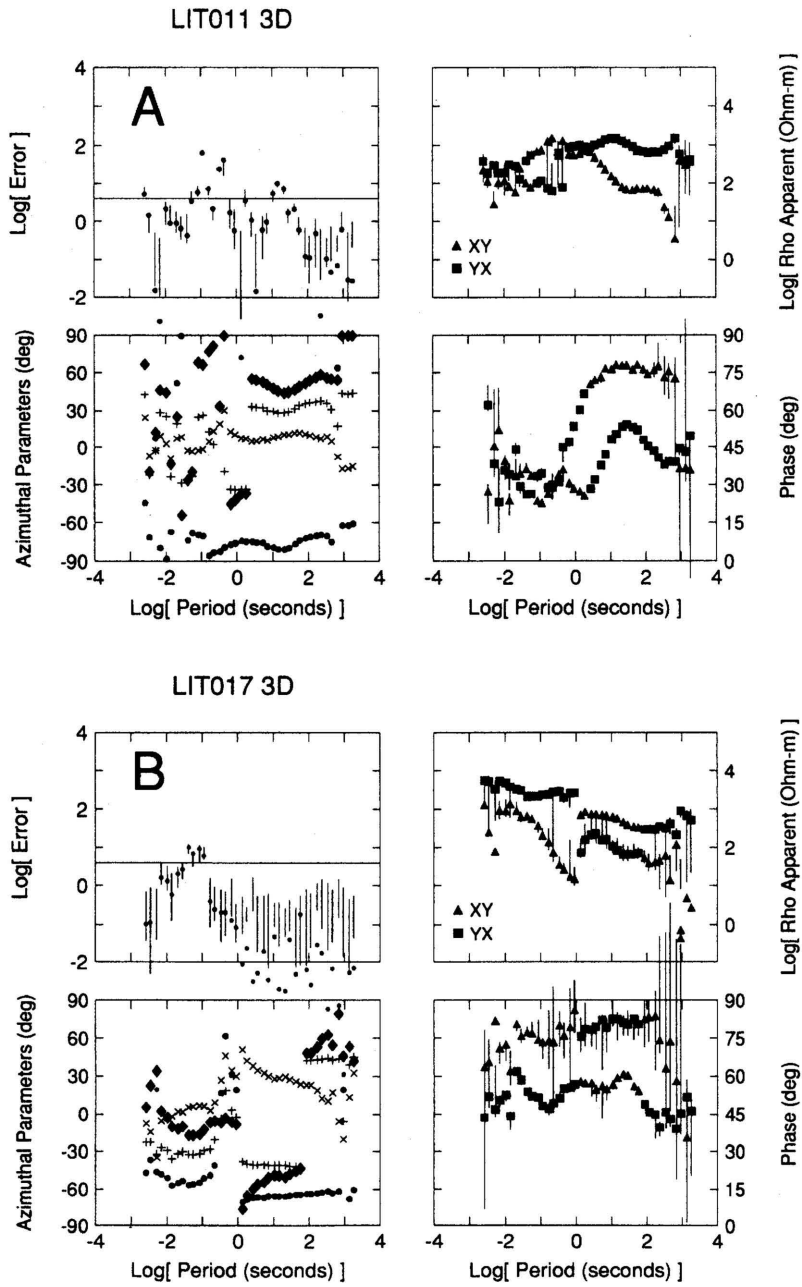
LIT011 3D

LIT017 3D

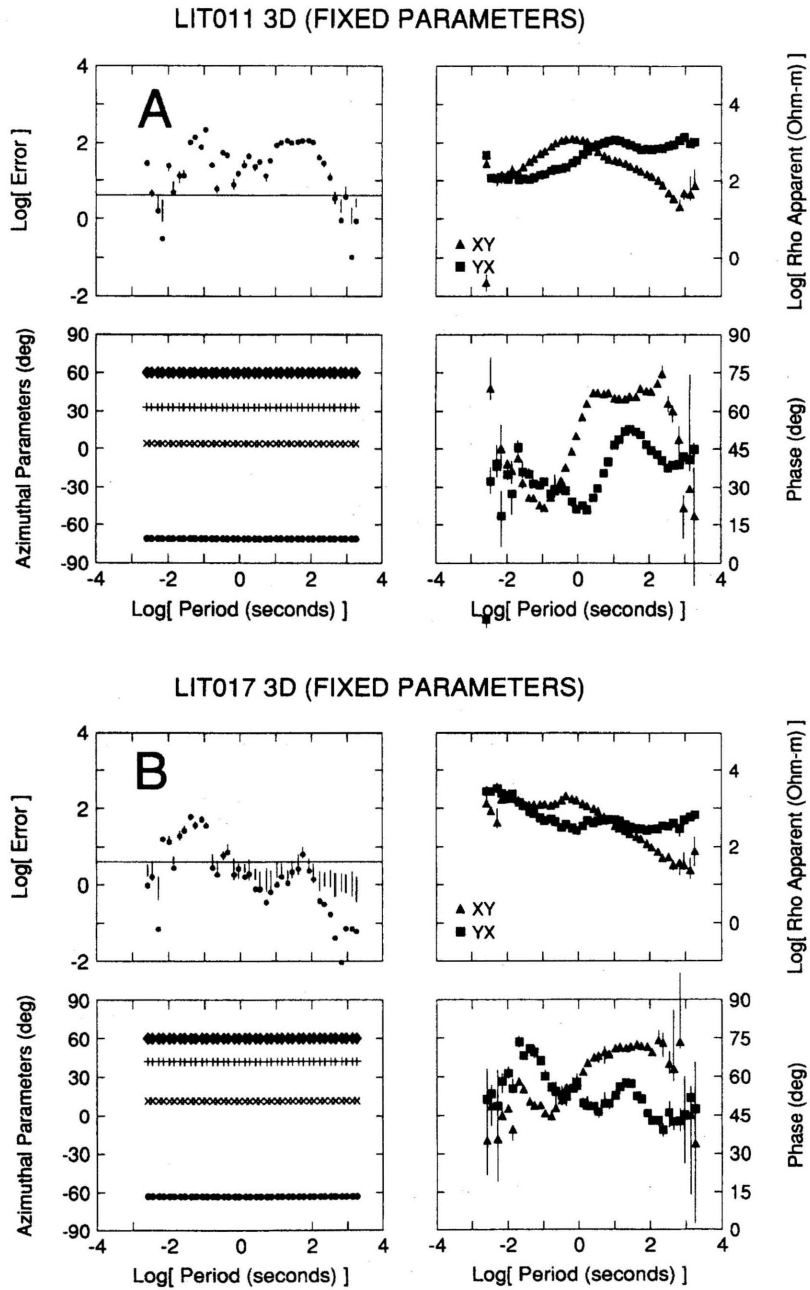Fig. 8. The GB unconstrained 3D/2D model parameters for sites *lit011* (A) and *lit017* (B).

Fig. 9. The final constrained 3D/2D GB parameters for sites *lit011* (A) and *lit017* (B).
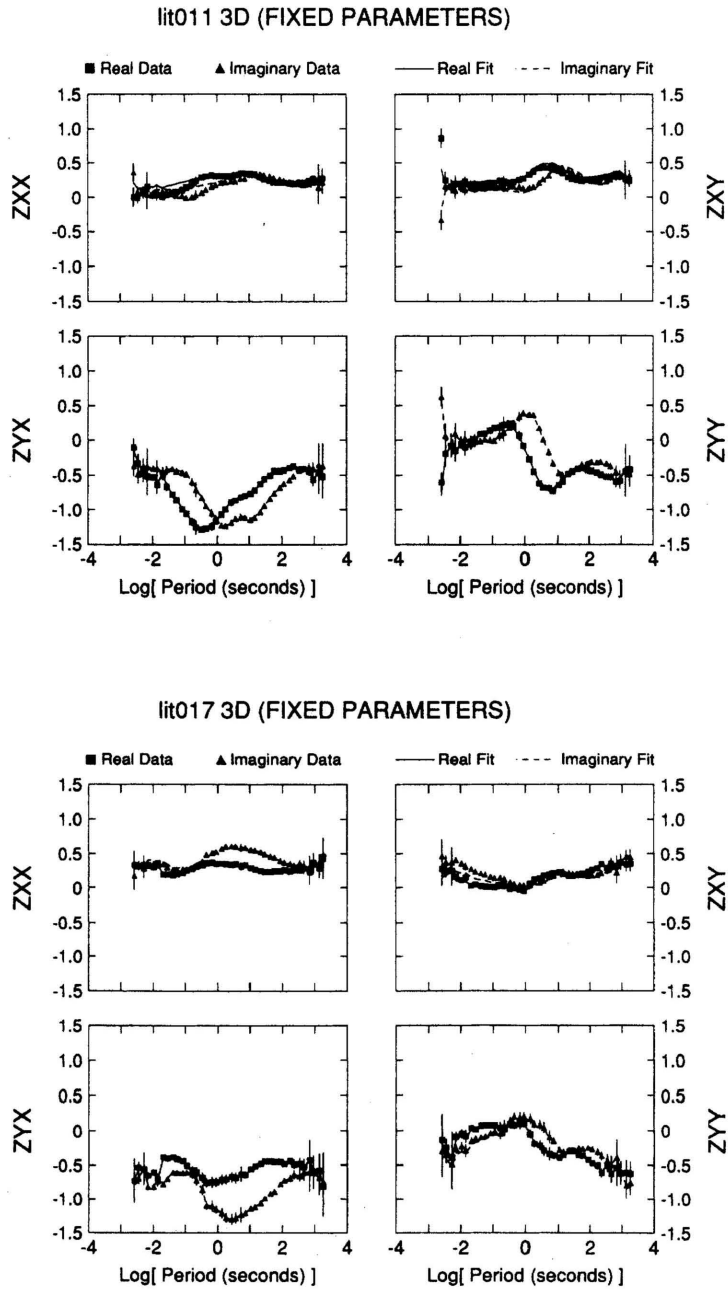
A. G. JONES *et al.*

lit011 3D (FIXED PARAMETERS)

■ Real Data   ▲ Imaginary Data   —— Real Fit   - - - Imaginary Fit

Fig. 10.   The fits of the constrained 3D/2D GB parameters for sites *lit011* (upper four plots) and *lit017* (lower four plots).
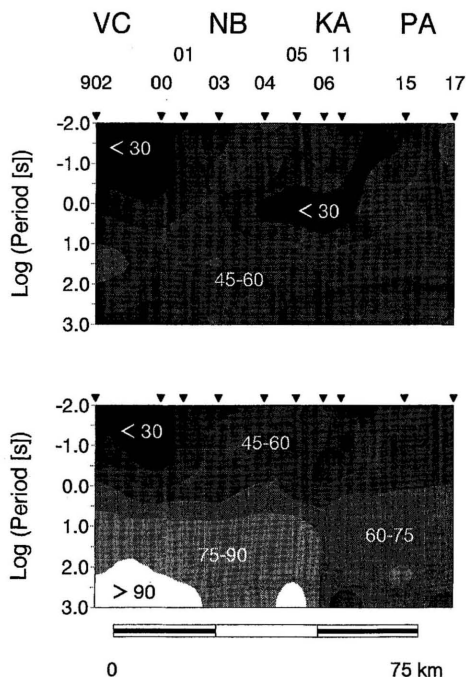
Fig. 11. Phase pseudosections of the decomposed ϕ_{xy} (top) and ϕ_{yx} (bottom) phases in strike co-ordinate system, with x pointing at $-30°$, for a reduced set of responses. The contour interval is $15°$; black regions denote phases below $30°$, whereas white regions denote phases greater than $90°$.

The resulting phases from a reduced set are shown in Figs. 11a and 11b, and are to be compared with the raw data in Figs. 1a and 1b. The data from these sites were chosen for modelling based on their stability, quality, and scatter. The phase associated with the B-polarization mode (Fig. 11b) is now more stable, both spatially and with period, compared with Fig. 1b. In addition, it is well-behaved in that there are no longer responses above $90°$ at periods less than 100 s. The E-polarization phase (Fig. 11a) is extremely uniform at long periods across the entire profile with a phase in the range $45°–60°$. To be noted in both figures are the low phase responses to the west of the Nelson Batholith (between site *902* and *00*), and the low phase over the Purcell Anticlinorium (between sites *11* and *15*) apparently dipping beneath the Kootenay Arc. The B-polarization phases (Fig. 11b) at long periods are uniformly high ($>60°$) over the entire profile.

The apparent resistivities, after GB decomposition, represent scaled versions of the true regional apparent resistivities. The two scale factors, or static shifts, at each site are reduced to one, the local site gain g, by shifting the two curves at each site so as to bring them together, thereby correcting for near surface anisotropy (GROOM and BAHR, 1992). Comparison of the data at this point with EMAP (see below), shows that the levels are very close to those expected for regional values, and the E-polarization responses indicate generally smooth amplitude progression across the profile GROOM and BAHR, 1992).

Figure 12 shows the E-polarization (*squares*) and B-polarization (*circles*) ρ_a data at 100 s from the sites in a reduced set as a function of lateral distance from site *lit000*. Note that whereas the B-polarization data range over almost two orders of magnitude, the E-polarization data range over only three-quarters of an order of magnitude, from 325 Ω·m to 1,750 Ω·m, with a weak increasing eastwards trend. A straight-line regression was fit (solid line, Fig. 12) to the
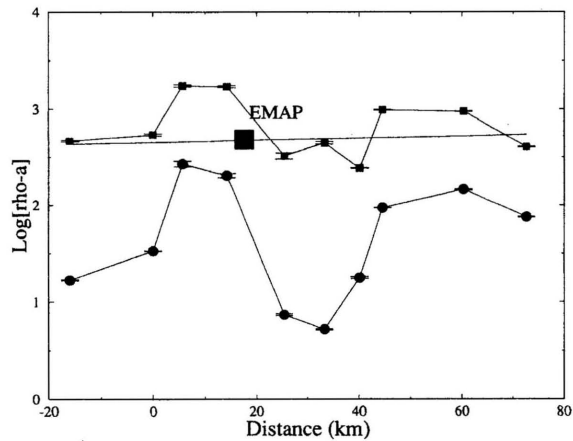
Fig. 12.   E-polarization (*squares*) and B-polarization (*circles*) ρ_a values at a period of 100 s, for the ten sites chosen for interpretation, as a function of position eastwards from site *lit000*. A first-order regression line through the E-polarization data, to which all E-polarization curves were shifted, is also shown (*solid line*). The *square* marked **EMAP** is the apparent resistivity value at 100 s from the zero wavenumber response from a north-south EMAP line.

E-polarization data, which gave a low correlation coefficient (0.16) between the ten values and their locations. The slope of the regression line is small, equivalent to 4 Ω·m/km, with 830 Ω·m at the eastern end reducing to 460 Ω·m at the western end. The null hypothesis of zero correlation, i.e., that a mean value is appropriate, can only be rejected at the 40% level of significance, which indicates that we cannot be confident of an increasing apparent resistivity eastwards. However, evidence for a required lateral variation in the data comes from the phase responses (Fig. 11a), which exhibit higher phases to the west decreasing to the east, in accord with an increasing resistivity.

We have undertaken an EMAP survey on the Nelson batholith with a total profile length of 10 km aligned NNW-SSE (JONES *et al.*, 1989). This line is oriented such that the response is equal to the E-polarization regional response. The zero-wavenumber response (JONES *et al.*, 1989) at a period of 85 s is 470 Ω·m; which is also plotted on Fig. 12 in approximately the correct lateral position. This zero-wavenumber EMAP value should be little affected by local distortions (GROOM and BAILEY, 1989b), and its coincidence with the regional trend supports our level assumption. A full frequency comparison of this EMAP response to a corrected neighbouring site highlights these points (GROOM *et al.*, 1993).

Accordingly, in order to apply the site gains, we shifted both ρ_a curves at each site such that the E-polarization curve lay on the regression line shown in Fig. 12 at 100 s period.

5.   Modelling

5.1   General comments

Two features in the data, after decomposition, were difficult to model; these are illustrated in Fig. 13 which displays the corrected data for site *lit006*. The large phase difference between the two modes in the period range 1–10 s, marked as **1** on Fig. 13, could not be modelled, nor could the parallel phase responses in the 10–100 s range, marked as **2**. The former characteristic was common for sites on the Nelson Batholith while the latter was consistent across the entire profile.
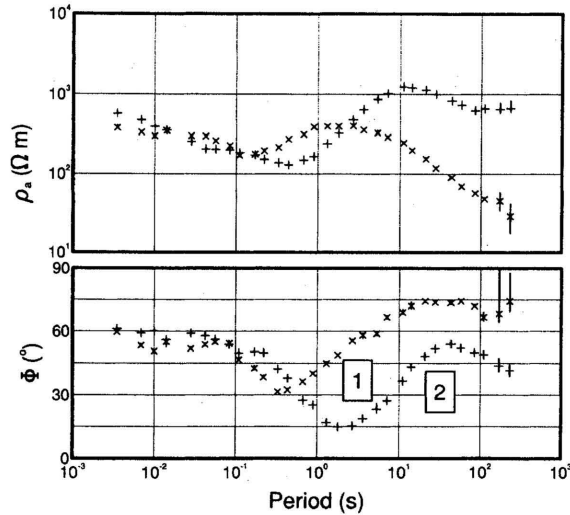
Fig. 13. Corrected, decomposed, MT regional responses from site *lit006*; the E-polarization data are shown as *pluses*, whereas the B-polarization responses are shown as *crosses*, together with one standard error estimates. Two aspects difficult to model are the large phase mode separation in the 1–10 s range (**1**), and the phase-parallel mode responses in the 10–100 s band (**2**).

We attribute the former to 3D effects caused by the Nelson batholith and other large-scale features. 3D modelling studies of an L-shaped lower crustal conductor, such as is inferred by the work of LAJOIE and CANER (1970: see Fig. 6 in JONES, 1993) gave about 10° phase difference between the two modes in the 1–10 s period band, but not the 35° observed (JONES *et al.*, 1993). At periods in excess of 10 s, these features have only a galvanic response.

As discussed below, we are only able to fit the latter type of phase behaviour (10–100 s) if we introduce a layer in our model that has a different resistivity in the two directions of polarization.

We undertook an extensive 2D forward modelling exercise, testing various features of the models, but to date only a limited 2D inversion of the data. We report on both here to illustrate the general confirmation that we obtained from the latter with regard to certain features in the model derived by the former.

5.2 2D forward modelling

These data were modelled using Wannamaker's (WANNAMAKER *et al.*, 1985) code (as implemented in the GEOTOOLS© package). The top 50 km of the model that best describes the gross features of the dataset is illustrated in Fig. 14; the anisotropic layer continues to a depth of 70 km, below which is an 1000 $\Omega \cdot$m layer to 400 km, then a 1 $\Omega \cdot$m half-space. The top 5 km of the model is shown above with a vertical exaggeration of 5:1 to illustrate the near-surface features. Also shown on the figure is the approximate trace of the Slocan Lake Fault (**slf**). The field data and model data are compared in Figs. 15 (apparent resistivities) and 16 (phases).

The principle features of this model are:

1. The Nelson batholith is modelled as a 20,000 $\Omega \cdot$m body with a 4 km depth extent. The location and geometry of its western boundary were taken from the seismic information; there is little control in the MT responses for its shape.
2. The Nelson batholith is bounded to the east by a zone of enhanced conductivity (50 $\Omega \cdot$m). The data are unequivocal about the existence of this feature, which also dominates the transfer function responses at around 1 s (see JONES *et al.*, 1988).
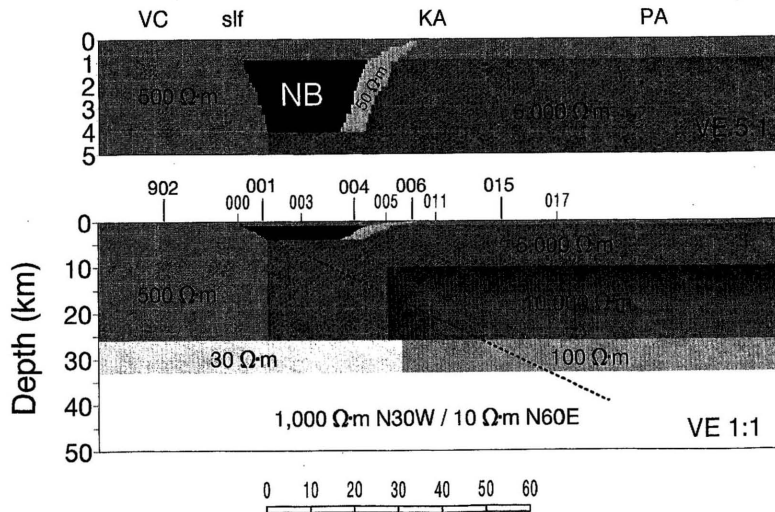
Fig. 14. Final two-dimensional model which best describes most of the gross features in the regional MT responses. The uppermost 5 km is illustrated with a vertical exaggeration of 5:1 on the upper figure, whereas the whole crustal model on a 1:1 exaggeration on the lower figure. The trace of the Slocan Lake Fault (slf), imaged by the seismic reflection profiles, is shown as the dashed line on the lower figure. Note the anisotropic upper mantle layer, with 1,000 Ω·m in the direction N30°W and 10 Ω·m in the direction N60°E.

3. There is a contrast in conductivity on either side of the Slocan Lake Fault in the mid- and lower crust. The highly resistive 10,000 Ω·m mid-crustal layer to the east we associate with North American cratonic basement; the lower crust here is modelled to be of some 70 S (7 km thick layer of 100 Ω·m), which is in accord with typical values for lower crustal conductance (JONES, 1992). To the west is modelled a 500 Ω·m layer to 26 km depth, underlain by a thin (7 km) layer of 30 Ω·m. The existence of the conducting lower crust was previously shown by JONES et al. (1988).

4. The upper mantle is modelled as electrically anisotropic, with 1,000 Ω·m in the N30°W direction (E-polarization direction), and 10 Ω·m in the N60°E direction (B-polarization direction). Figure 17 shows the phase responses for the model with a 1,000 Ω·m upper mantle layer (Fig. 17A) and with a 10 Ω·m layer (Fig 17B). Note that the former fits the long period ϕ_{xy} phases, but not the ϕ_{yx} ones, whereas the latter fits the ϕ_{yx} long period phases but not the ϕ_{xy} ones. We were unable to find a 2D model that fit both long period phases which did not include an anisotropic layer. Such an anisotropic mantle layer has been proposed for eastern regions of Canada beneath the Canadian Shield (KELLETT et al., 1992; KURTZ et al., 1993).

5.3 2D inversion

In order to make the 2D inversion tractable, and to try to fit as much of the dataset as possible, the inversion proceeded in stages. The data inverted were from the reduced set of ten sites whose phase responses are shown in Fig. 11. As discussed above with regard to the error estimates, we could not be confident that the small estimates in the dead-band would not bias the model in their favour over information at other periods. Accordingly, we assumed an error level of 5% of the impedance elements for all data (5% in impedance is equivalent to ≈10% in apparent resistivity and ≈2.9° in phase). Both MT modes were used for inversion, but not the GDS responses. DEGROOT-HEDLIN and CONSTABLE's (1990) Occam2 was used for inversion
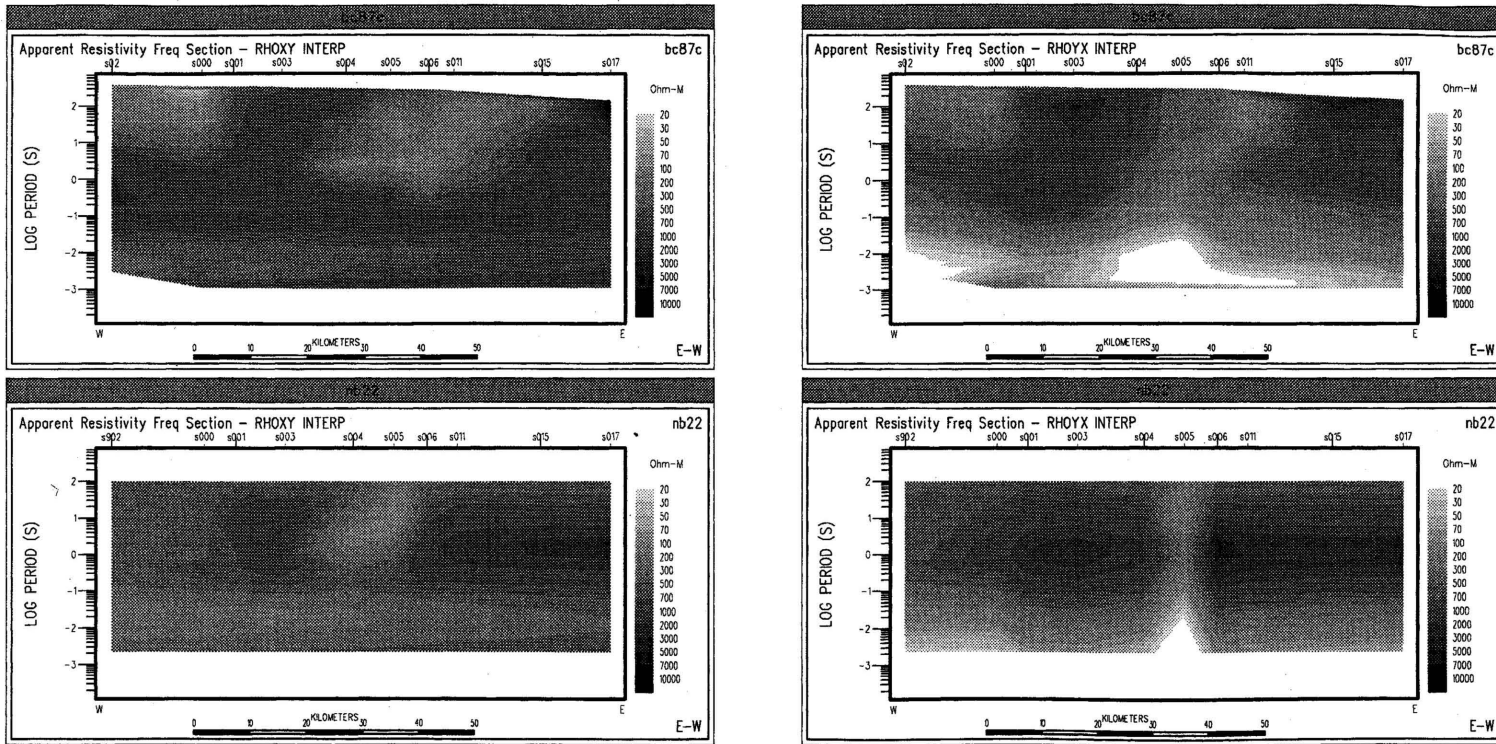
Fig. 15. Comparison of field and model apparent resistivity data for the model illustrated in Fig. 14. The top two pseudosections are the field data, whereas the bottom two are the modelled data. The left column gives the E-polarization responses, whereas the right column gives the B-polarization ones.
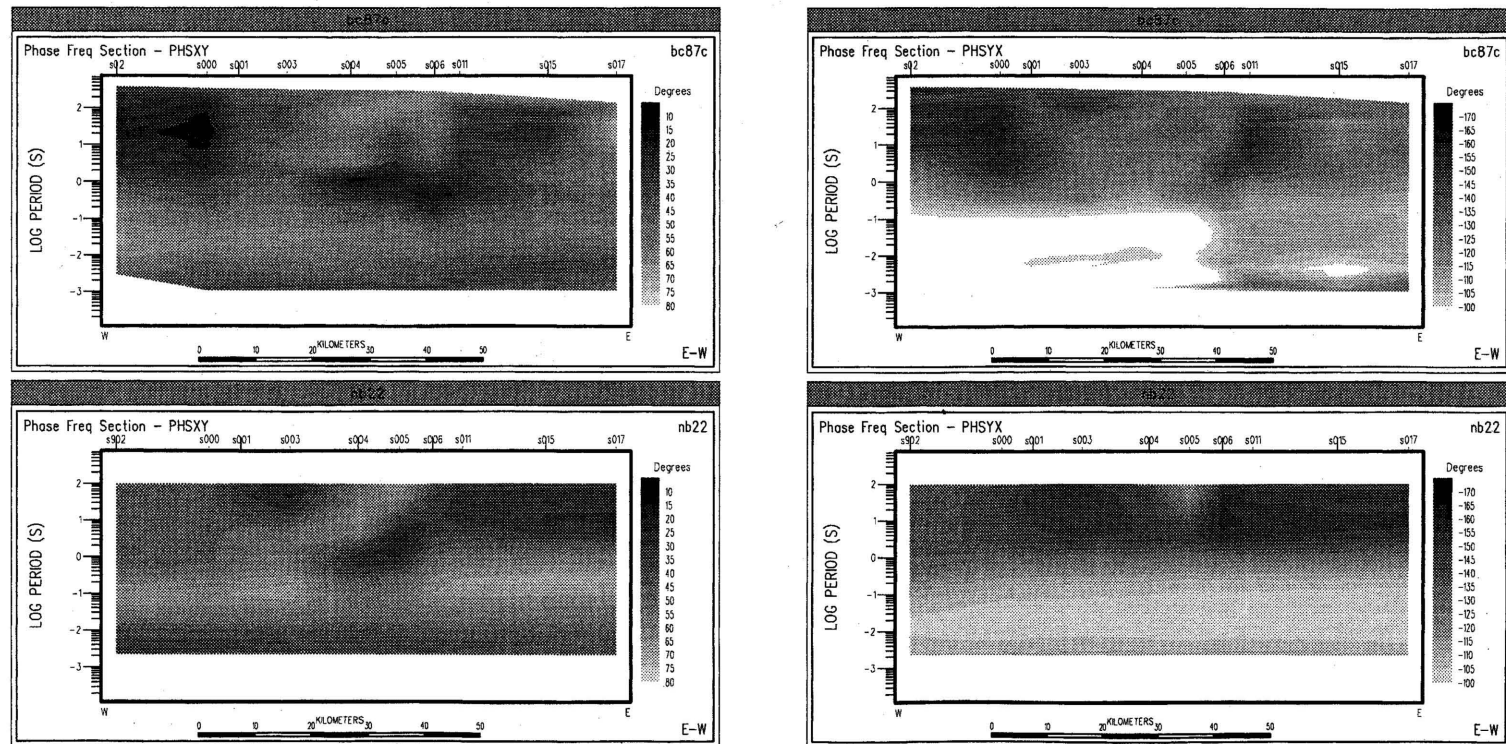
Fig. 16. Comparison of field and model phase data for the model illustrated in Fig. 14. The top two pseudosections are the field data, whereas the bottom two are the modelled data. The left column gives the E-polarization responses, whereas the right column gives the B-polarization ones.
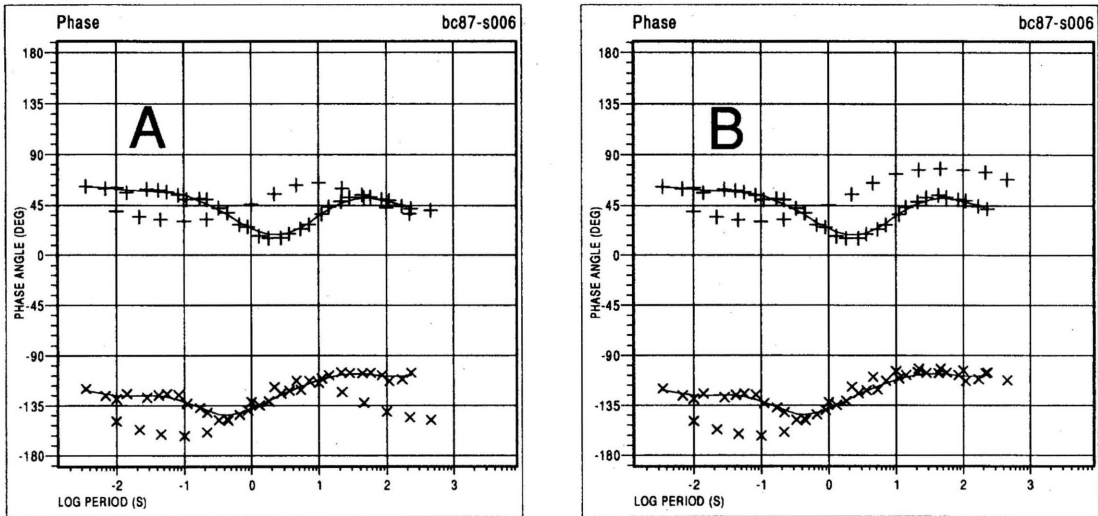
Fig. 17. The E-polarization (*pluses*) and B-polarization (*crosses*) phases from site *lit006* compared to the model responses with an upper mantle of 1,000 Ω·m (**A**) and of 10 Ω·m (**B**) (the data are the symbols joined by the two lines). Note that the former fits the E-polarization phase data in the period range 10–100 s, but not the B-polarization data; and conversely for the latter.

(implemented as part of the GEOTOOLS© package).

A half-space model was used as the start model, with 28 regularization grids horizontally, and 25 vertically, with decreasing horizontal grids with depth. The model ended with a half-space at a depth of 60 km. The total number of free regularization blocks was 600. In the first stage, a best-fitting model was sought which fit all data in the range 10–100 Hz from both modes at all ten sites, i.e., 280 data (7 freqs, 10 sites, 2 modes, ρ_a and ϕ). With assumed errors of 5% in impedance, the smallest RMS misfit possible was 3.04, with a roughness of 18.4. Accordingly, the smoothest model with an RMS misfit of 3.25 was then sought; this model has a roughness value of 3.7.

Having found a smooth model which fit the highest frequency band responses, the top 4 km of the model was held fixed for the second stage; this reduced the number of free parameters from 600 to 521. At this point, a best-fitting model was sought which fit all data in the range 1–10 Hz from both modes at all ten sites, i.e., 280 data. This model had an RMS of 2.78 and a roughness of 13.7. The smoothest model was then sought which had an RMS of 3.0; its roughness was 0.76.

The top 12 km of the model was held fixed for the next two stages of the inversion. This reduced the number of free parameters to 381. Due to the strong inductive 3D effects considered present in the data within the range 1–10 s, no attempt was made to fit them.

In the third stage, the best fitting model was sought which fit the E-polarization mode data only in the range 10–100 s, i.e., 140 data. This model had an RMS of 1.0, which was the target, with a roughness of 0.9.

In the fourth stage, the best fitting model was sought which fit the B-polarization mode data only in the range 10–100 s, i.e., 140 data. This model had an RMS of 5.04, with a roughness of 390.8. A smooth model with an RMS misfit of 5.5 was then sought; it has a roughness of 28.7.

The two models shown in Fig. 18 illustrate those found from the above inversion strategy. With such a large misfit to the B-polarization mode data, the model only fits the phases to within 15° on average, and the misfit residuals are serially correlated. Accordingly, we consider these
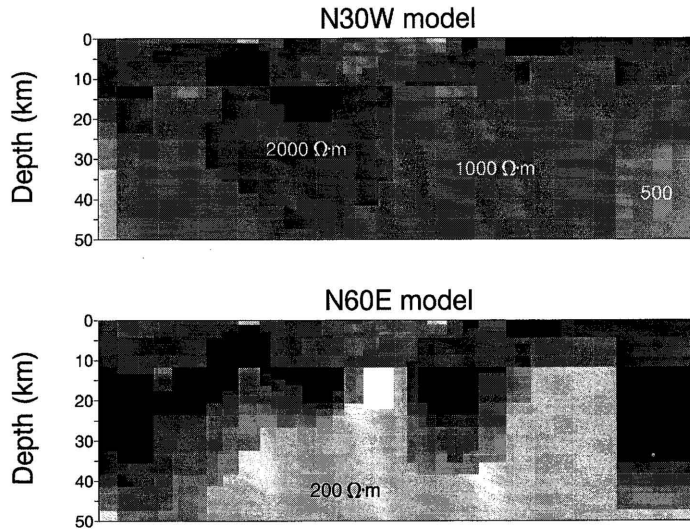
Fig. 18.   The two 2D models found using Occam2 inversion with a vertical exaggeration of 1:1 (see text for details); *top model* fits high frequency data (>1 Hz) and E-polarization data in the range 10–100 s; *bottom model* fits high frequency data (>1 Hz) and B-polarization data in the range 10–100 s. Contour interval is 1/3 of a decade, from 100 Ω·m (*white*) to 5,000 Ω·m (*black*).

models preliminary, and are attempting to find models which fit the data better. However, three features in the models confirm those in the forward model. The resistive Nelson batholith, and a conducting region beneath the sites on its eastern boundary, are evident, and the E-polarization data indicate a highly-resistive mantle, of greater than 1,000 Ω·m, whereas the B-polarization data support an upper mantle an order of magnitude more conducting. There appears to be little support in these inversions for a laterally-varying middle and lower crust despite the ubiquitous presence of well-determined E- and B-polarization responses, which are different in both phase magnitude and amplitude shape, at relevant periods.

6.   Discussion and Conclusions

The MT data in the BC87 dataset are highly complex and require modern distortion analyses to derive regional responses for which a 2D interpretation is valid. We chose to use the GB approach, and have illustrated its use on the data from some of the sites. Having corrected for phase-distortion, the levels of the ρ_a curves must be set. This we did by requiring a smooth variation across the survey area in our E-polarization long-period ρ_a data. Our analyses indicate that the data in the band 1–10 s are affected by large-scale 3D induction effects. This period band is that for which the Nelson batholith phases are severely distorted, and thus we conclude that within this band structures of the horizontal scale-size, not vertical scale-size, of the batholith, i.e., 150 × 50 km, are important.

The distortion- and level-corrected data were modelled using both 2D forward trial-and-error model fitting and objective 2D smooth inversion (Occam2). The resulting models show features which correlate with the surface geology, particularly the Nelson batholith and a conducting region on its eastern boundary. We associate this conducting region, which appears to bound the eastern side of the batholith, with Ag, Pb and Zn vein and replacement deposits of the Riondel (Bluebell) and Ainsworth camps thought to be remobilised from Lower Cambrian stratiform

Kootenay Arc deposits during batholith emplacement (DAWSON *et al.*, 1991). This feature also has a very strong vertical field response, as illustrated in Fig. 5 of JONES *et al.* (1988).

The inverse models (Fig. 18) do not appear to support the view that there is a strong contrast in conductivity on either side of the Slocan Lake Fault. However, we consider that the models derived from inversion preliminary, and further work on this issue must be undertaken. In particular, the forward modelling was subjectively weighted towards those data that we considered were more representative of the regional responses. For example, for some sites the data in the range 1–10 s were used, since we considered them free from 3D inductive effects, whereas all responses in this band were ignored in the inversions. Our knowledge of the effects of 3D structures (e.g., JONES, 1983; WANNAMAKER *et al.*, 1984) would suggest that we could validly invert the B-polarization responses, but not the E-polarization ones, and it is precisely the latter that gave us the greatest difficulties (see Fig. 17).

One major conclusion is the requirement for an anisotropic layer beneath the region. We place this layer in the upper mantle, rather than the lower crust, but the depth is not well constrained. The anisotropy factor is well over one order of magnitude, possibly as much as two. With analogy to seismic anisotropy, the "slow" direction is N60°E, whereas the "fast" direction is N30°W. It is perhaps significant that the former represents the Juan de Fuca plate-push direction. Given the noted high temperatures of the mantle in this region (GOUGH, 1986), one possible explanation is of stress-aligned cracks filled with partially-molten material. However, such a view is difficult to reconcile with the believed ductile rheology of the lower crust and uppermost mantle for this region (LOWE and RANALLI, 1993).

REFERENCES

BAHR, K., Elimination of local 3D distortion of the magnetotelluric tensor impedance allowing for two different phases, Contributed paper at 7th Workshop on Electromagnetic Induction in the Earth and Moon, held in Ile-Ife, Nigeria, on August 15–22, 1984.

CLOWES, R. M., F. A. COOK, A. G. GREEN, C. E. KEEN, J. N. LUDDEN, J. A. PERCIVAL, G. M. QUINLAN, and G. F. WEST, LITHOPROBE: new perspectives on crustal evolution, *Can. J. Earth Sci.*, **29**, 1813–1864, 1993.

DAWSON, K. M., A. PANTELEYEV, A. SUTHERLAND BROWN, and G. J. WOODSWORTH, Regional metallogeny, in *Geology of the Cordilleran Orogen in Canada*, edited by H. Gabrielse and C. J. Yorath, Geological Survey of Canada, Geology of Canada, No. 4, pp. 707–768, 1991.

DEGROOT-HEDLIN, C. and S. CONSTABLE, Occam's inversion to generate smooth two-dimensional models from magnetotelluric data, *Geophys.*, **55**, 1613–1624, 1990.

GOUGH, D. I., Mantle upflow tectonics and the Canadian Cordillera, *J. Geophys. Res.*, **91**, 1909–1919, 1986.

GROOM, R. W., The effects of inhomogeneities on magnetotellurics, Ph.D. Thesis, Publ. by Univ. Toronto, Research in Applied Geophysics Series, v. 42, 1988.

GROOM, R. W. and R. C. BAILEY, Decomposition of magnetotelluric impedance tensors in the presence of local three-dimensional galvanic distortion, *J. Geophys. Res.*, **94**, 1913–1925, 1989a.

GROOM, R. W. and R. C. BAILEY, Some effects of multiple lateral inhomogeneities in magnetotellurics, *Geophys. Prospect.*, **37**, 697–712, 1989b.

GROOM, R. W. and R. C. BAILEY, Analytical investigations of the effects of near-surface three-dimensional galvanic scatterers on MT tensor decomposition, *Geophys.*, **56**, 496–518, 1991.

GROOM, R. W. and K. BAHR, Corrections for near surface effects: decomposition of the magnetotelluric impedance tensor and scaling corrections for regional resistivities: a tutorial, *Surv. Geophys.*, **13**, 341–380, 1992.

GROOM, R. W., R. D. KURTZ, A. G. JONES, and D. E. BOERNER, A quantitative methodology for determining the dimensionality of conductive structure from magnetotelluric data, *Geophys. J. Int.*, 1993 (in press).

GROOM, R. W., A. G. JONES, and R. D. KURTZ, The electrical structure at the edge of cratonic North America—I. magnetotelluric data and decomposition analyses, *Geophys. J. Int.*, 1994 (in preparation).

JONES, A. G., The problem of "current channelling": a critical review, *Geophys. Surv.*, **6**, 79–122, 1983.

JONES, A. G., Electrical conductivity of the continental lower crust, in *Continental Lower Crust*, edited by D. M. Fountain, R. J. Arculus, and R. W. Kay, Chapter 3, pp. 81–143, Elsevier, 1992.

JONES, A. G., The BC87 dataset: tectonic setting, previous EM results, and recorded MT data, *J. Geomag. Geoelectr.*, this issue, 1089–1105, 1993.

JONES, A. G. and R. W. GROOM, Strike angle determination from the magnetotelluric tensor in the presence of noise and local distortion: rotate at your peril!, *Geophys. J. Int.*, **113**, 524–534, 1993.

JONES, A. G., R. D. KURTZ, D. W. OLDENBURG, D. E. BOERNER, and R. ELLIS, Magnetotelluric observations along the LITHOPROBE southeastern Canadian Cordilleran transect, *Geophys. Res. Lett.*, **15**, 677–680, 1988.

JONES, A. G., D. E. BOERNER, R. D. KURTZ, D. OLDENBURG, and R. ELLIS, EMAP data processing in the wavenumber domain, Contributed paper at 59th Annual Society of Exploration Geophysics meeting, held in Dallas, Texas, on 29 October–2 November, Abstract publ. in Conference Proceedings, **59**, 172–174, 1989.

JONES, A. G., D. I. GOUGH, R. D. KURTZ, J. M. DeLAURIER, D. E. BOERNER, J. A. CRAVEN, R. G. ELLIS, and G. W. McNEICE, Electromagnetic images of regional structure in the southern Canadian cordillera, *Geophys. Res. Lett.*, **12**, 2373–2376, 1992.

JONES, A. G., R. D. KURTZ, and R. W. GROOM, The electrical structure at the edge of cratonic North America—II. modelling, inversion, and tectonic implications, *Geophys. J. Int.*, 1994 (in preparation).

KELLETT, R. L., M. MARESCHAL, and R. D. KURTZ, A model of lower crustal electrical anisotropy for the Pontiac Subprovince of the Canadian Shield, *Geophys. J. Int.*, **111**, 141–150, 1992.

KURTZ, R. D., J. A. CRAVEN, E. R. NIBLETT, and R. A. STEVENS, The conductivity of the crust and mantle beneath the Kapuskasing Uplift: electrical anisotropy in the upper mantle, *Geophys. J. Int.*, **113**, 483–498, 1993.

LAJOIE, J. J. and B. CANER, Geomagnetic induction anomaly near Kootenay Lake—a strike-slip feature in the lower crust?, *Can. J. Earth Sci.*, **7**, 1568–1579, 1970.

LOWE, C. and G. RANALLI, Density, temperature, and rheological models for the southeastern Canadian Cordillera: implications for its geodynamic evolution, *Can. J. Earth Sci.*, **30**, 77–93, 1993.

WANNAMAKER, P. E., G. W. HOHMANN, and S. H. WARD, Magnetotelluric responses of three-dimensional bodies in layered earths, *Geophys.*, **49**, 1517–1533, 1984.

WANNAMAKER, P. E., J. A. STODT, and L. RIJO, PW2D: Finite element program for solution of magnetotelluric responses of two-dimensional Earth resistivity structure, Earth Science Laboratory, Univ. Utah Res. Inst., Salt Lake City, 1985.

ZHANG, P., L. B. PEDERSEN, M. MARESCHAL, and M. CHOUTEAU, Channelling contribution to tipper vectors: a magnetic equivalent to electrical distortion, *Geophys. J. Int.*, **113**, 693–700, 1993.